Influence of increased greenhouse gases and sulphate aerosols concentration upon diurnal temperature range over Africa at the end of the 20th century

C. Caminade[1] and L. Terray[1]

Received 22 March 2006; revised 30 May 2006; accepted 12 June 2006; published 1 August 2006.

[1] In order to investigate the diurnal temperature range response under enhanced greenhouse gases and sulphate aerosols concentrations over Africa, two ensembles of 19 integrations are conducted using the ARPEGE climate model. The ensembles are forced with the same observed changes in sea surface temperature and sea-ice extents but differ in terms of the anthropogenic direct effect included. When accounting for the additional anthropogenic effect due to the direct radiative forcing, diurnal temperature range significantly decreases during the last two decades of the 20th century over Africa. Over North and Southern Africa, this decrease is related to a significant increase of minimum temperatures mainly due to the additional greenhouse effect. Over West Africa, an increase of cloud albedo causes the daily maximum temperature to decrease resulting in a weakening of the diurnal temperature range. Simulated diurnal temperature range is then compared to the observed one to assess confidence in the results. **Citation:** Caminade, C., and L. Terray (2006), Influence of increased greenhouse gases and sulphate aerosols concentration upon diurnal temperature range over Africa at the end of the 20th century, *Geophys. Res. Lett.*, *33*, L15703, doi:10.1029/2006GL026381.

1. Introduction

[2] The diurnal temperature range (DTR) is a relevant indicator of climate change, that is due to the asymmetry between maximum and minimum temperature response to anthropogenic forcing [*Braganza et al.*, 2004]. Several studies highlight a significant decreasing trend in the DTR at global scale [*Vose et al.*, 2005; *Easterling et al.*, 1997; *Jin and Dickinson*, 2002; *New et al.*, 2000]. The large increase of minimum daily temperatures compared to a much smaller enhancement of maximum temperatures over land is responsible of such global DTR changes. Nevertheless, strong regional differences in mean DTR changes have been highlighted [*Vose et al.*, 2005]. For example, the DTR increases in some regions (northeastern Canada, southern Argentina, eastern Africa, the western Pacific ocean and southeastern Australia) whereas it decreases elsewhere. Previous works showed that DTR variations are strongly related to variations in cloud cover [*Dai et al.*, 1997, 1999; *New et al.*, 2000], soil moisture [*Durre et al.*, 2000; *Dai et al.*, 1999], the ground albedo and ground heat capacity [*Stone and Weaver*, 2003].

[3] The African continent experienced a significant warming (about 0.5°C) during the 20th century [*Hulme et al.*, 2001]. Six of the observed warmest years occurred during the last two decades. Only a few studies have examined long term changes of the DTR over Africa, mainly due to the lack of observations over this continent. Over Sudan and Ethiopia mean annual DTR have decreased by between 0.5°C and 1°C since the 1950's whereas over Zimbabwe the DTR significantly decreases during the 50's and the 60's and remains stable until now [*King'uyu et al.*, 2000; *Hulme et al.*, 2001].

[4] The purpose of this work is first, using numerical experiments, to highlight the direct or immediate anthropogenic impact (as opposed to that which has arisen via oceanic feedbacks) upon minimum and maximum temperatures over Africa during the monsoon period (July–August–September or JAS) to improve the understanding of the associated physical mechanisms. Then, a comparison is done between the model DTR response and recent available observations from CRU [*Mitchell and Jones*, 2005].

[5] The paper is presented as follows: section 2 describes briefly the model and the experimental setup. Section 3 is devoted to the impact of an additional anthropogenic forcing in the model framework and the associated physical mechanisms. Section 4 compares mean DTR changes as simulated by the model and the available observations. Finally, the last section gives a summary and some perspectives.

2. Model and Experimental Design

[6] The Météo-France ARPEGE model version employed in this study is described in detail by *Déqué et al.* [1994]. The model uses a semi-lagrangian advection scheme, a two time level discretization, a 30 min step, the spectral truncation is T63 and there are 31 vertical levels. The radiative forcing includes the effect of 4 greenhouse gases or GHG (CO2, CH4, N2O and CFC) in addition to water vapour and ozone and of five aerosol types (organic and black carbon, sea salt, desert dust and sulphates). Two 19 member ensemble simulations are performed over the period 1950–1999. Within each ensemble, the simulations only differ by their initial conditions. The first ensemble (CPi) is forced by observed monthly SST [*Smith and Reynolds*, 2004], GHG and sulphate (SUL) concentrations being fixed to their pre-industrial values (1900). A second ensemble (CSi) is then performed to quantify the direct radiative impact of enhanced GHG and SUL concentrations upon the African climate system. GHG concentrations are

[1]Climate Modelling and Global Change Team, URA 1875, Centre Européen de Recherche et de Formation Avancée en Calcul Scientifique, CNRS, Toulouse, France.

0094-8276/06/2006GL026381$05.00

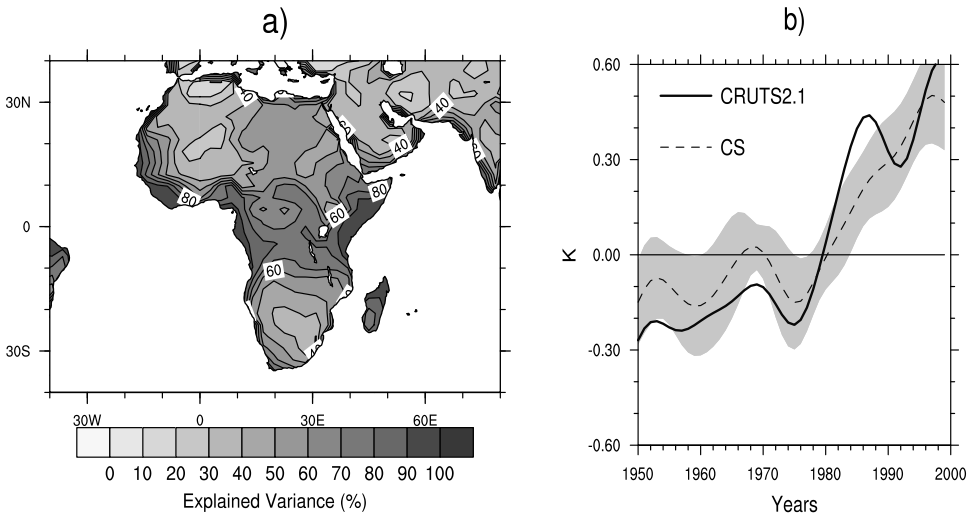

Figure 1. (a) Percentage of the variance of decadal temperature due to the SST plus anthropogenic forcing over the period 1951–1999 (JAS), based on the CSi ensemble. All displayed values significantly exceed zero at the 1% significance level. (b) Temperature anomalies with respect to the 1961–1990 average during JAS over Africa for the CRUTS2.1 data set (bold solid line), and CS (dashed line) ensemble mean. The gray filled area depicts the spread (defined as two standard deviations of the 19 simulations with respect to the ensemble mean) in the CSi ensemble. The data are low pass filtered with a 10 year cut-off.

yearly varying and the seasonal cycle of SUL concentration is updated decade by decade using the Boucher data set [*Boucher and Pham*, 2002]. The others aerosols are kept constant (CPi and CSi) and the indirect effect of SUL is not implemented in the model. Note that all natural and anthropogenic external forcing are partly included in the imposed observed SST. In this study, only the additional direct radiative effect (due to the GHG and SUL concentrations increase in the atmosphere) is characterized and will be referred hereafter as "anthropogenic forcing". The CPi (CSi) ensemble mean gives an estimator of the SST (SST + anthropogenic) forced signal which will be referred as to CP (CS) in the following.

3. Model Response to Anthropogenic Forcing

3.1. Mean Changes

[7] A spectral analysis of variance (ANOVA) [see *Rowell and Zwiers*, 1999] is applied to the CSi ensemble to quantify the fraction of the variance of JAS temperature due to oceanic and anthropogenic forcing against the internal variability of the atmosphere (Figure 1a). At decadal time scale, the percentage of JAS temperature variance due to the external forcing (also referred as potential predictability or PP) is relatively high (about 90%) over the coastal area (Guinea, Cameroon, Gabon, Somalia coast) and Central Africa. This high PP can be explained by the direct continental temperature response of the nearby SST. Over North and Southern Africa the PP is about 50%. The PP significantly (slightly) increases by about 20% over Southern Africa when accounting for the additional anthropogenic forcing (not shown). Considering all frequencies the ANOVA pattern is not modified, the only significant change is in term of amplitude (the PP is reduced by about 10%).

[8] At decadal time scale, the observed temperature remains stable over the 1950–1979 period and significantly warms up (by about 0.5°C) during the 80's and the 90's (Figure 1b). The model (CSi) reproduces this warming trend that occurred during the last two decades. Simulated temperatures are warmer (cooler) than observed ones over the 1950–1979 (1980–1999) period. In terms of interannual variability, the average of the correlations between all simulated (CSi) and observed Africa temperature indices is 0.6 with a standard deviation of 0.1, (the data have been high-pass filtered with an 8 year cut-off, and the results are significant at the 0.1% significance level as estimated by a Student t-test). In the following, the analysis is focused on the last two decades of the 20th century, because the African continent experienced a significant temperature increasing trend.

[9] CS minus CP mean temperature change pattern exhibits an enhancement of temperature over North and Southern Africa (Figure 2a). A slight cooling can be noticed over West Africa. The additional impact of the anthropogenic forcing upon the DTR results in a decrease over the whole African domain (with no significant changes over East Africa and the Guinea coast area) during the last two decades (Figure 2b). The DTR decrease can be primary related to the strong increase of minimum temperature (Tmin, Figure 2c) over the North and Southern Africa (and no significant changes over the sub-Saharan area), and the significant decrease of maximum temperature (Tmax, Figure 2d) over West Africa (with a small non significant increase over the Sahara and Southern Africa). Attention is focused on these specific areas where mean Tmin and Tmax change patterns strongly differ: the North African (NA), the West African (WA) and South African (SA) regions (see Figure 2). An extended investigation of the physical mechanisms responsible for such Tmin and Tmax changes is performed in the following sections.

3.2. Statistical Analysis

[10] A step-wise regression method (forward selection and backward elimination algorithm [see *Von Storch and*

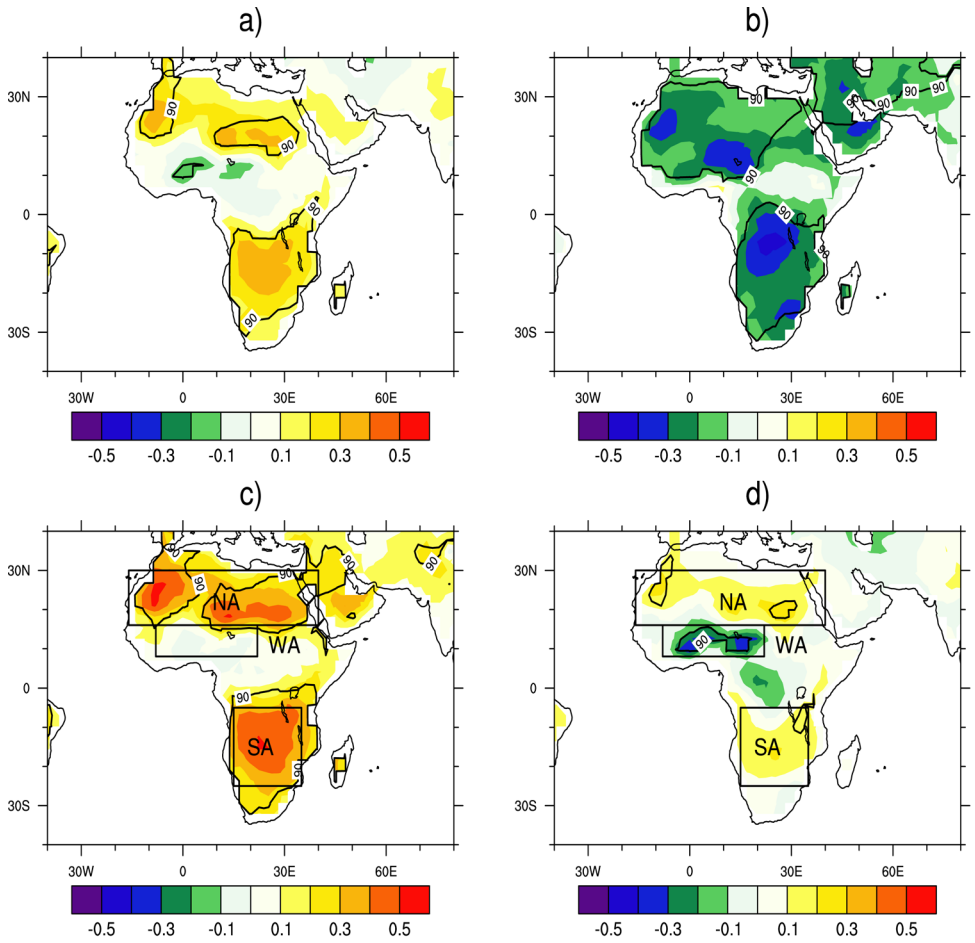

Figure 2. CS - CP mean (a) temperature, (b) DTR, (c) Tmin and (d) Tmax changes (K) during JAS over the 1980–1999 period. Black contour line denotes significant differences at the 10% significance level as estimated by a student t-test.

Zwiers, 1999]) is applied to CS to determine the best predictors of Tmin, Tmax and DTR over the different domains (Table 1). Based on previous work, six predictors are selected: the longwave downwelling radiation at the surface (LWd), latent and sensible heat flux (LatF and SensF), the cloud liquid water content (Cl_{liq}), the total atmospheric vapour water content (Vtot), and Cloud cover (Cl_{cov}). Changes in mean daytime solar radiation (SWd) are not considered as they are assumed to be implicitly included in (Cl_{cov}) and (Cl_{liq}) ones. Soil moisture is not considered as it is assumed to be closely linked to the latent heat flux (through surface evaporation). The predictor time series are built by averaging over the predictand regions previously defined, and are high pass filtered with a 8 year cut-off. The significance level for including or removing a variable from the regression equation is fixed at the 0.1% level. If the multiple linear correlation coefficient reached the threshold of 0.90 the implicated predictor(s) is(are) then retained.

[11] Over NA, Tmin is significantly correlated with LWd. Tmax can be accurately estimated only considering LWd and SensF variations. Over WA, strong linear links are highlighted between minimum temperature, LWd and cloud properties. Moreover, significant correlation coefficients are denoted between Tmax, cloud properties and the LWd over this domain. Focusing on the SA domain, Vtot (LWd) is significantly correlated with the DTR (Tmin). As a summa-

Table 1. Correlations Between Tmin, Tmax, the DTR and Different Physical Parameters Over the Period 1950–1999 During JAS (CS)[a]

	Tmin	Tmax	DTR
NA	LWd (0.98)[b] Tot (0.98)[b]	LWd (0.71)[b], SensF (0.53)[b] Tot (0.95)[b]	LWd (−0.53)[b], SensF (0.87)[b] Tot (0.96)[b]
WA	LWd (0.83)[b], Cl_{cov} (−0.52)[c] Tot (0.95)[b]	Cl_{liq} (−0.70)[b], Cl_{cov} (−0.81)[b], LWd (0.47)[c] Tot (0.96)[b]	Cl_{liq} (−0.87)[b], Cl_{cov} (−0.87)[b] Tot (0.95)[b]
SA	LWd (0.96)[b], Tot (0.96)[b]	LWd (0.77)[b], Vtot (0.62)[c] Tot (0.93)[b]	Vtot (−0.92)[b] Tot (0.92)[b]

[a]The Tot variable is the multiple linear correlation coefficient.
[b]Denotes significant correlations at the 1% significance level as estimated by a random phase test [*Ebisuzaki*, 1997].
[c]Denotes significant correlations at the 5% significance level as estimated by a random phase test [*Ebisuzaki*, 1997].

Table 2. CS - CP Mean Changes During JAS Over the Period 1980–1999 for Different Physical Parameters[a]

CS - CP	LWd, W/m^2	SWd, W/m^2	LatF, W/m^2	SensF, W/m^2	Cl_{liq}, 10^{-3}g/kg	Cl_{cov}, %	Vtot, g/kg	SUL, mgS/m^2	Tmin, K	Tmax, K	DTR, K
NA	3.77[b]	−3.89[b]	0.42[c]	−0.34	0.20	−0.07	0.46	4.05	0.35[b] (0.38)	0.10 (0.18)	−0.25[b] (−0.19)
WA	1.55[c]	−3.76[b]	1.90[c]	−2.10[c]	4.26[c]	0.32	0.70[c]	2.10	0.08 (0.11)	−0.21[d] (−0.17)	−0.29[b] (−0.24)
SA	3.00[b]	−1.70[b]	0.44	−0.28	0.35	0.29	0.24	0.30	0.34[b](0.38)	0.08 (0.14)	−0.26[b] (−0.22)

[a]Predicted changes for DTR, Tmin and Tmax using the regressions with the retained predictors of Table 1 are displayed in parentheses.
[b]Denotes significant changes at the 1% significance level as estimated by a Student t-test.
[c]Denotes significant changes at the 5% significance level as estimated by a Student t-test.
[d]Denotes significant changes at the 10% significance level as estimated by a Student t-test.

ry, over NA and SA, LWd is closely linked with DTR variations whereas over WA cloud properties depict significant correlations with the DTR. The linear links highlighted here for CS are not modified in CP.

3.3. Physical Mechanisms

[12] Table 2 shows mean changes between CS and CP experiment over the 1980–1999 period (JAS) for different physical parameters. Over NA, the DTR significantly decreases due to the large increase of Tmin. The downward longwave radiation at the surface is enhanced (related to the GHG increase) and causes Tmin to increase. During daytime, the strong increase of LWd is counterbalanced by the strong decrease in shortwave downward radiation. The SWd decrease can be related to the scattering effect of SUL over this area as the mean SWd change pattern is spatially correlated with CS-CP difference in SUL forcing (not shown).

[13] Tmax changes are strongly linked to cloud properties over WA. An increase of GHG concentration causes the cloud liquid water content to increase over WA. There is no significant modification of cloud cover. However, increase in Cl_{liq} changes the cloud optical thickness, enhancing cloud albedo and thus decreasing SWd. This cloud optical thickness negative feedback on surface temperature has been shown in past studies [*Somerville and Remer*, 1984]. It serves as a thermostat to stabilize the climate against changes in long-wave radiative forcing. The Cl_{liq} enhancement results in an increase of rainfall over WA and so in an increase of surface evaporation that amplifies the surface cooling (this link is not displayed in Table 1 as the effect of LatF is accounted for by Cl_{liq} over this specific region). Thus, the Tmax decrease is due to both an increase of cloud albedo, an enhanced surface evaporative cooling, and partially to an increase of SUL concentration. Nevertheless, the cloud albedo effect upon Tmax seems to be predominant over this domain (not shown). The LWd increase and so Tmin change is much smaller over WA than NA and SA.

[14] Over SA, mean Tmin changes are driven by the same physical mechanism previously denoted over NA. No consistent physical mechanism is proposed here to explain the slight Tmax increase.

4. Consistency of the Results

[15] Are the simulated DTR changes coherent with the available observations over Africa? Figure 3 depicts DTR anomalies over the three domains of interest for the CRUTS2.1 data set [*Mitchell and Jones*, 2005], CPi and CSi ensemble. Note that the CRUTS2.1 observed data set employed here is not optimized for climate change detection studies. The station network being very sparse, a spatio-temporal mask consistent with the station network is applied to the simulations.

[16] Over NA very few observations are available (not shown). The available stations are mainly located over eastern Sudan, North of Egypt, North of Niger and Mali. A DTR decreasing trend is depicted in the observations (Figure 3a). The model reproduces the DTR decreasing trend (CPi and CSi), despite a clear underestimation. Whereas positive observed DTR anomalies are depicted over the 1950–1960 period, the simulated DTR range shows slight negative ones. During the last two decades, simulated DTR time evolution agrees better with the observed one when accounting for an additional anthropogenic forcing.

[17] Over WA, there are no available observations during the 50's, and the number of station decreases during the 90's (not shown). The observed DTR remains quite stable during the 60's and the 70's and decreases over the 1985–1999 period (Figure 3b). The model reproduces this behaviour, but there are no significant differences between CS and CP during the 80's, suggesting that the SST forced signal in driving DTR variability is predominant here. The CS minus CP mean DTR changes (denoted in section 2) is mainly due to differences that occurred during the second part of the 90's.

[18] Finally, over SA, the station network is dense over the 1950–1995 period and decreases thereafter (not shown). The observed DTR slightly decreases during the 50's and the 60's, and remains stable until 1999. In the CPi and CSi ensemble the DTR remains stable over the whole period in agreement with the observed one. Note that year 1999 is omitted in the analysis here as very few stations are available over SA leading to a spatial homogeneity problem related to a bias in the simulated DTR representation.

[19] When only accounting for SST external forcing (CPi), a significant DTR decreasing trend is depicted over the regions of interest. The significant warming of the Tropical Atlantic ocean that occurred during the last two decades is suggested to cause this DTR decrease through enhanced humidity transport over the western part of NA (causing Tmin to decrease through a LWd increase), and enhanced precipitation over the Gulf of Guinea and the southern part of WA (causing Tmax to decrease through cloud albedo increase).

5. Conclusion and Discussion

[20] The DTR significantly decreases over Africa during JAS over the 1980–1999 period. When only accounting for

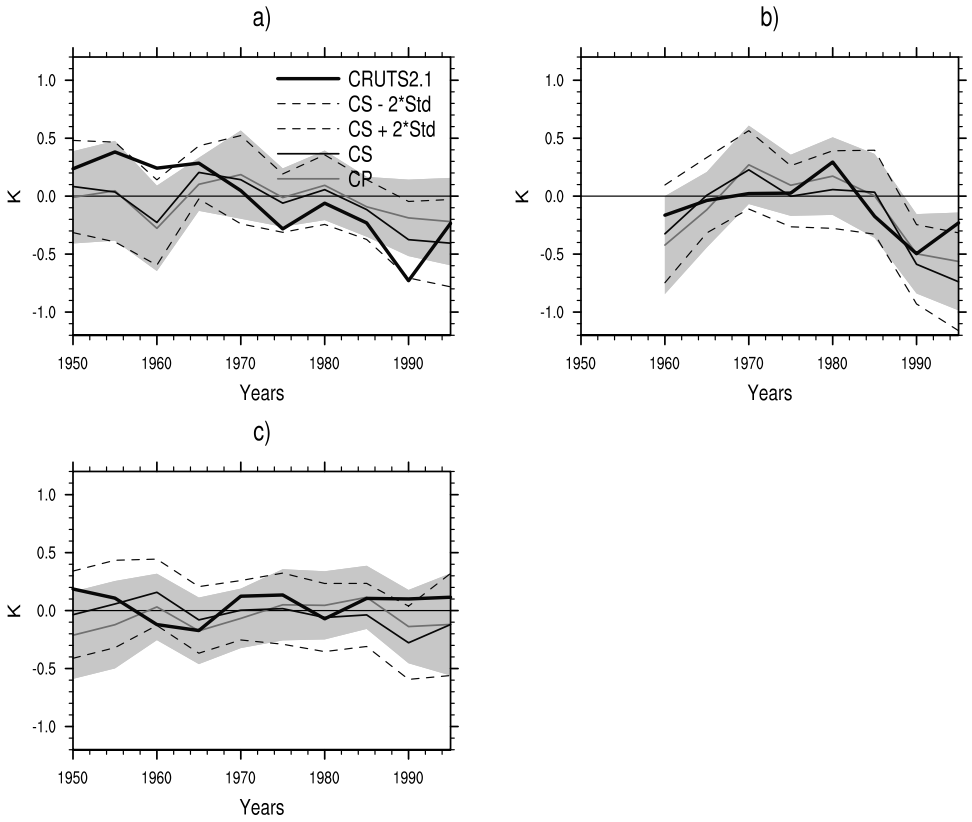

Figure 3. 5 year means of DTR anomalies (with respect to the 1961–1990 climatology) during JAS over (a) NA, (b) WA and (c) SA for the CRUTS2.1 data set (bold solid line), CP (solid gray line) and CS (solid black line). The gray filled area (dashed lines) depicts the spread (defined as two standard deviations of the 19 simulations with respect to the ensemble mean) in the CPi (CSi) ensemble.

SST external forcing, the model reproduces part of this DTR decreasing trend. Under enhanced GHG and SUL atmospheric concentrations, this DTR decrease is more pronounced suggesting that the direct anthropogenic forcing is emerging from the noise over this period. It amplifies the Tmin decrease (through a LWd increase related to the additional greenhouse effect) over North and Southern Africa. Moreover it leads to an additional decrease of Tmax over WA (through an increase of cloud albedo). Nonetheless, the experimental set-up employed in this study lacks extra-forcings shown to be predominant over Tropical Africa. First, carbonaceous aerosols time evolution is not included in the direct radiative forcing added in CSi although its impact upon the radiative budget over Africa is important (through biomass burning). Moreover, the volcanic forcing is not considered here. Then, as suggested by *Stone and Weaver* [2003], the importance of soil moisture implies that change in land use and vegetation properties may have an impact on the DTR (not considered here). As a perspective, an ocean-atmosphere coupled approach (including more feedbacks) will be a natural extension of this work in order to highlight the mechanisms responsible for DTR changes over Africa.

[21] **Acknowledgments.** This work was supported by the French AMMA-API project and by the European Community via the sixth framework ENSEMBLE project under contract GOCE-CT-2003-505539. We thank Tim Mitchell for providing the CRUTS2.1 data set.

References

Boucher, O., and M. Pham (2002), History of sulfate aerosol radiative forcings, *Geophys. Res. Lett.*, *29*(9), 1308, doi:10.1029/2001GL014048.

Braganza, K., D. J. Karoly, and J. M. Arblaster (2004), Diurnal temperature range as an index of global climate change during the twentieth century, *Geophys. Res. Lett.*, *31*, L13217, doi:10.1029/2004GL019998.

Dai, A., A. D. Del Genio, and I. Y. Fung (1997), Clouds, precipitation and temperature range, *Nature*, *386*, 665–666.

Dai, A., K. E. Trenberth, and T. R. Karl (1999), Effects of clouds, soil moisture, precipitation and water vapor on diurnal temperature range, *J. Clim.*, *14*, 485–519.

Déqué, M., C. Dreveton, A. Braun, and D. Cariolle (1994), The climate version of Arpege/IFS: A contribution to the French community climate modeling, *Clim. Dyn.*, *10*, 249–266.

Durre, I., J. M. Wallace, and D. P. Lettenmaier (2000), Dependance of extreme daily maximum temperatures on antecedent soil moisture in the contiguous United States during summer, *J. Clim.*, *13*, 2641–2651.

Easterling, D. R., et al. (1997), Maximum and minimum temperatures trends for the globe, *Science*, *277*, 364–367.

Ebisuzaki, W. (1997), A method to estimate the statistical significance of a correlation when the data are serially correlated, *J. Clim.*, *10*, 2147–2153.

Hulme, M., R. Doherty, T. Ngara, M. New, and D. Lister (2001), African climate change: 1900–2100, *Clim. Res.*, *17*, 145–168.

Jin, M., and R. E. Dickinson (2002), New observational evidence for global warming from satellite, *Geophys. Res. Lett.*, *29*(10), 1400, doi:10.1029/2001GL013833.

King'uyu, S. M., L. A. Ogallo, and E. K. Anyamba (2000), Recent trends of minimum and maximum surface temperatures over Eastern Africa, *J. Clim.*, *13*, 2876–2886.

Mitchell, T. D., and P. D. Jones (2005), An improved method of constructing a database of monthly climate observations and associated high-resolution grids, *Int. J. Climatol.*, *25*, 693–712.

New, M., M. Hulme, and P. Jones (2000), Representing twentieth-century space-time climate variability. part II: Development of 1901–96 monthly grids of terrestrial surface climate, *J. Clim.*, *13*, 2217–2238.

Rowell, D. P., and F. W. Zwiers (1999), The global distribution of sources of atmospheric decadal variability and mechanisms over the tropical Pacific and southern North America, *Clim. Dyn.*, *15*, 751–772.

Smith, T. M., and R. W. Reynolds (2004), Improved extended reconstruction of SST (1854–1997), *J. Clim.*, *17*, 2466–2477.

Somerville, R. C. J., and L. A. Remer (1984), Cloud optical thickness feedbacks in the CO_2 climate problem, *J. Geophys. Res.*, *89*(D6), 9668–9672.

Stone, D. A., and A. J. Weaver (2003), Factors contributing to diurnal temperature range trends in twentieth and twenty-first century simulations of the CCCma coupled model, *Clim. Dyn.*, *20*, 435–445.

Von Storch, H., and F. W. Zwiers (1999), *Statistical Analysis in Climate Research*, Cambridge Univ. Press, New York.

Vose, R. S., D. R. Easterling, and B. Gleason (2005), Maximum and minimum temperature trends for the globe: An update through 2004, *Geophys. Res. Lett.*, *32*, L23822, doi:10.1029/2005GL024379.

C. Caminade and L. Terray, Climate Modelling and Global Change Team, CERFACS, 42 Av. Gaspard Coriolis, F-31057 Toulouse Cedex 01, France. (caminade@cerfacs.fr)